I&EC research
Industrial & Engineering Chemistry Research

pubs.acs.org/IECR

Article

# Energy Lost in a Hydrogel Osmotic Engine Due to a Pressure Drop

Tri Quang Bui, Vinh Duy Cao, Wei Wang, Thanh Hung Nguyen, and Anna-Lena Kjøniksen*

Cite This: https://doi.org/10.1021/acs.iecr.1c00409

Read Online

ACCESS | Metrics & More | Article Recommendations

**ABSTRACT:** Utilizing hydrogels to harvest salinity gradient energy from solutions of different salinities has recently attracted interest. Polyelectrolyte hydrogels exhibit cyclic swelling/deswelling when alternately exposed to freshwater and seawater. This can be utilized to convert the mixing energy of the two solutions into mechanical energy. Hydrogels consisting of a semi-interpenetrating network (semi-IPN) of poly(4-styrene sulfonic acid-*co*-maleic acid) sodium salt and polyacrylic acid was prepared at various cross-linking densities. The energy lost due to a pressure drop in the system during the deswelling/swelling process of these hydrogels is examined, and the effects of tubing dimensions, hydrogel cylinder size, gel particle size, and the volume fraction within the hydrogel cylinder occupied by the flowing liquid ($\varepsilon$) are investigated. In addition, a small-scale osmotic engine was compared to a scaled-up system. $\varepsilon$ was found to be the factor that had the largest effect on the energy loss. It was found that $\varepsilon$ is strongly dependent on the degree of swelling of the hydrogels. When the hydrogels swell, they deform more easily under pressure. This markedly decreases $\varepsilon$, thereby inducing a high pressure drop in the system and a correspondingly large energy loss. Accordingly, the pressure drop when pumping through the hydrogel is the major contributor to the energy loss in the system. When the hydrogel particles deform too much, the energy needed to pump the flowing liquid through the hydrogels exceeds the energy produced by the system. Developing a hydrogel system that deforms less in its swollen state is therefore essential for improving the energy efficiencies of these osmotic engines.

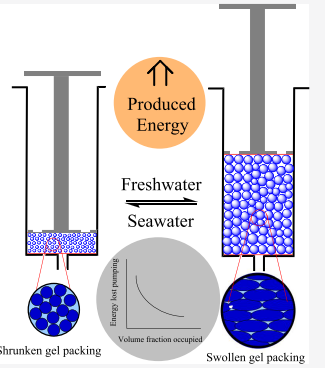




## 1. INTRODUCTION

Replacing fossil energy with clean and affordable energy sources[1−4] that reduce greenhouse gas emissions[5,6] is essential to avoid global warming. Salinity gradient energy is generated when solutions with different salinities are mixed.[7] The salinity gradient energy when river water flows into the ocean has been estimated to equal to a 200 m-high waterfall.[8] Globally, this corresponds to more than 1 TW, enough to cover 1% of the energy demand on the planet.[9−11]

In 1954, Pattle[8] demonstrated the hydroelectric pile, which was the first apparatus to harvest electricity directly from mixing seawater and fresh water. In the hydroelectric pile, the seawater and freshwater flows were separated by acidic and basic membranes, and the current was led off at the end of the pile. In the 70s, Norman and Loeb[7,12] proposed a theoretical model based on the thermodynamic osmotic pressure of seawater. The fresh water and seawater were separated by a semipermeable membrane in a pressure chamber. An infinitesimal volume of water would flow from the freshwater reservoir into the pressure chamber and spill off the top of the water column. This water could then produce electricity through a waterwheel and a generator. However, this technique was uneconomical with a high cost of the produced electricity.

Recently, salinity gradient power generation technologies have been developed based on the concepts of Pattle and Norman[7,8] These include pressure-retarded osmosis (PRO),[9,13−17] where the difference in chemical potential generates a flow through a semipermeable membrane and feeds a hydro-turbine to produce electricity; reverse electrodialysis (RED),[18−23] where electricity is generated by ion flux owing to the different ion concentrations at the ion-exchange membranes; and capacitive mixing (CapMix),[24−28] which works as an electrochemical double-layer capacitor.

The alternative of using hydrogels to convert salinity gradient energy into mechanical energy was introduced by Zhu *et al.* in 2014.[29] High and low salinity solutions alternatingly flow through a hydrogel, which is placed in a modified syringe that is operating in a piston-type process. The expansion and contraction of the hydrogel in aqueous solutions of different salinities transform the chemical potential energy into mechanical energy.

Recently, various polyelectrolyte hydrogels have been tested for their energy-generating potential.[29−33] The recovered energies per gram of dried hydrogel have been reported as up to 3.4 J/g for poly(allylamine hydrochloride),[30] 102 J/g for polysulfobetaine,[32] 0.83 J/g for poly(acrylic acid),[31] 9.5 J/g for

Received: January 28, 2021
Revised: June 25, 2021
Accepted: July 6, 2021

poly(acrylic acid-*co*-vinylsulfolnic acid),[33] and 13.3 J/g for poly(4-styrenessulfonic acid-*co*-maleic acid) interpenetrated in a poly(acrylic acid) network.[33] It is however important to note that the utilized osmotic engine will also affect the recovered energy. Most studies focus on the energy recovered from the system, and the energy lost during the cycling process has not been explored for lab-scale energy production systems. Zhang *et al.*[34] discussed the pressure drop of the supply pump for a small system, utilizing poly(styrene sulfonate sodium salt) hydrogels. The results indicated that the energy loss due to pumping was much smaller than the work output. This is essential for achieving an overall energy production from the system. In this study, we explore how the tubing dimensions, hydrogel cylinder sizes, gel particle sizes, and volume fractions within the hydrogel cylinder occupied by the flowing liquid ($\varepsilon$) affect the energy lost to the pressure drop of two osmotic engines of different sizes. An empirical equation for estimating how $\varepsilon$ varies with the degree of swelling of the hydrogels was developed. The utilized hydrogels are chosen based on their superior performance in a recent study[33] and are semi-interpenetrating networks of poly(4-styrene sulfonic acid-*co*-maleic acid) sodium salt and poly(acrylic acid) at various cross-linker concentrations. Semi-interpenetrating networks exhibit superior mechanical properties compared to traditional hydrogels,[35] which is important for their ability to swell against external pressure to generate salinity gradient energy.

## 2. MATERIALS AND METHODS

**2.1. Materials.** Acrylic acid (AA), *N*′,*N*′-methylenebis-(acrylamide) (MBA), ammonium persulfate (APS), *N*,*N*,*N*′,*N*′-tetramethylethylenediamine (TEMED), and poly-(4-styrene sulfonic acid-*co*-maleic acid) sodium salt (PSSA-MA) with an average molecular weight of 20,000 g/mol were purchased from Sigma-Aldrich and used as received.

**2.2. Synthesis of Semi-IPN PAA-PSSA Gels.** Stock solutions were prepared by mixing 2.5 g of acrylic acid monomers and 1 g of PSSA-MA in 20 mL of distilled water. TEMED (0.24 mL, 25% aqueous solution), APS (0.04 g), and the MBA cross-linker (0.08, 0.16, and 0.21 g) were consecutively added to the solution under stirring. The resulting hydrogels have molar cross-linking concentrations of 1.5, 3.0, and 4.0%, which were labeled as PAA-PSSA1.5, PAA-PSSA3.0, and PAA-PSSA4.0, respectively. The mixtures were purged with nitrogen gas for 10−20 min, and the stock solutions were sealed with aluminum foil. In order to activate the APS radical initiator, gelation was carried out in an oven at 50 °C. Since the gelation reaction proceeds faster with increasing cross-linker concentration, the samples were kept in the oven for 120 min (1.5% cross-linker), 60 min (3.0% cross-linker), and 40 min (4.0% cross-linker) to form the hydrogels. After gelation, the hydrogels were cut into small pieces and immersed in a large quantity of deionized water to remove unreacted monomers and catalysts. The water for dialysis was changed daily for 15−20 days in order to reach equilibrium swelling for the hydrogels.

Since the MBA cross-linker does not react with the PSSA-MA polymer, the resulting PAA-PSSA hydrogels are semi-interpenetrating networks (semi-IPN) of poly(4-styrene sulfonic acid-*co*-maleic acid) sodium salt (PSSA-MA) and poly(acrylic acid) (PAA). In water (pH 7), the carboxylic groups in PAA partially dissociate ($K_a = 5.6 \times 10^{-5}$), whereas the sulfonic acid dissociates completely ($K_a = 2 \times 10^{-1}$).[36,37] The charged groups generate strong repulsive forces within the hydrogel, causing a high swelling capacity. Introducing sulfonic acid groups in PAA hydrogels is therefore expected to significantly improve the swelling ratio of the hydrogels. The presence of maleic acid in the copolymer structure increases the compatibility of PSSA-MA in the PAA network due to a similar structure of maleic acid and acrylic acid. In addition, the presence of the maleic acid anion reduces the formation of hydrogen bonds between polyacrylic acid chains due to its bulky structure and its electrostatic charge. This results in an increasing swelling ratio of the hydrogel.

**2.3. Harvesting Energy from Salinity Gradients Using Hydrogels.** Hydrogels can swell or deswell when immersed in aqueous solutions of different salinities. Exchange of both ions and water molecules between the gel and the surrounding water changes the salt concentration of both. Consequently, mixing energy is released. This energy is transformed into a change of volume and pressure of the hydrogel. Part of the mixing energy is converted into elastic energy within the hydrogel during swelling (low salinities). This elastic energy is stored in the hydrogel and later released during deswelling (high salinities).[34] Accordingly, we have a process that is reversible when the hydrogels are exposed to low and high salinity solutions. When the exchange of water and ions reaches equilibrium, the maximum available mixing energy is achieved, and the swelling volume of the hydrogels becomes constant.

Zhang *et al.*[34] demonstrated that the net change of Gibbs free energy of mixing during one deswelling/swelling cycle corresponds to the released mixing energy between the high and low salinity solutions, with no net change in the free energy of the gel (which starts and ends in the same state). Accordingly, hydrogels can convert the mixing energy of two solutions of different salinities into mechanical energy without changing its own energy state. The total free energy of mixing ($E_{mix}$) can be expressed as[29]

$$E_{mix} = RT \sum \left( V_{HC} c_{i,HC} \ln \frac{\alpha_{i,HC}}{\alpha_{i,M}} + V_{LC} c_{i,LC} \ln \frac{\alpha_{i,LC}}{\alpha_{i,M}} \right) \quad (1)$$

where $V$ and $c$ are the volume and concentration of ions of the aqueous solutions, respectively. The subscripts indicate high concentration (HC), low concentration (LC), and concentration of the mixed solution (M). $\alpha_{i,HC}$, $\alpha_{i,LC}$, and $\alpha_{i,M}$ are the activities of the ionic species $i$ in the HC solution (saltwater), LC solution (freshwater), and mixed solution, respectively.

The mixing energy can be recovered from the expansion and contraction of the hydrogels by utilization of an osmotic engine. A small-scale osmotic engine for investigating the mechanical energy recovered from the hydrogels is shown in Figure 1. A syringe with a diameter of 4.2 cm was placed vertically, and the saline solutions were pumped into the gel from the bottom to the top. Holes were drilled through the bottom of the plunger to facilitate the flow of water. The holes were covered by small cloths to prevent the hydrogel from being pressed through the holes. The swelling of the hydrogel is limited to changes in height since the cylinder walls prevent expansion in other directions.

The cylinder tube was filled with 60 mL of hydrogel that had been swollen in pure water until it reached a steady state (see Figure 2 for the corresponding swelling ratios). A weight was applied on the top of the plunger, providing a pressure ($p_L$) of 36.1 kPa. The high salinity solution was pumped through the


https://doi.org/10.1021/acs.iecr.1c00409
Ind. Eng. Chem. Res. XXXX, XXX, XXX−XXX

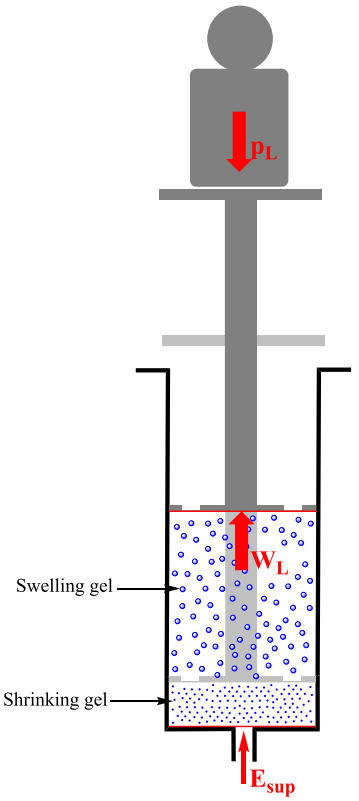


**Figure 1.** Small-scale osmotic engine. Water with high or low salinity is supplied from the bottom. The pumping energy ($E_{sup}$) is supplying water into the cylinder, where the swelling of the hydrogel conducts work ($W_L$) by lifting the external load, and $p_L$ is the pressure of the external load.

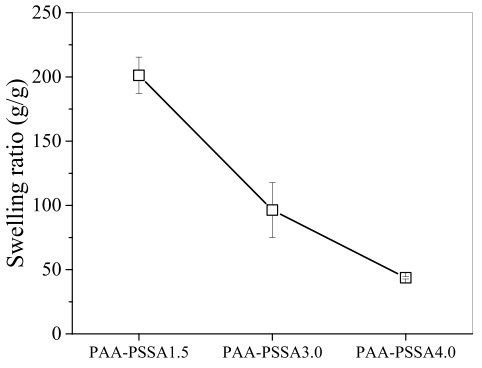


**Figure 2.** Effect of cross-linking concentration on the swelling ratio of PAA-PSSA hydrogels.

gel at a rate of 3 mL/min from the bottom of the tube until the plunger reached its lowest position where the hydrogel obtained its shrinking volume ($V_{sh}$). Then, the deionized water was pumped through with a flow at a rate of 5 mL/min. This causes the hydrogel to swell until it reaches its maximum swelling volume ($V_{sw}$). Each cycle (shrinking and swelling) lasted for 1 h. The total recovered energy can be expressed as the work ($W_L$) of one cycle:

$$W_L = p_L(V_{sw} - V_{sh}) \tag{2}$$

The work ($E_{pump}$) performed by the pump that flushes the water through the hydrogels can be expressed as[32]

$$E_{pump} = p_L Q_{sh} t_{sh} + p_L Q_{sw} t_{sw} \tag{3}$$

where $Q$ is the volumetric flow rate, $t$ is the time, and the subscripts sw and sh refer to the swelling and shrinking processes, respectively. The total energy supplied into the system ($E_{sup}$) is

$$E_{sup} = E_{mix} + E_{pump} \tag{4}$$

The percentage efficiency ($\eta_{\%}$) of energy recovered by the system compared to the mixing energy and the energy supplied by the pump is

$$\eta_{\%} = \frac{W_L}{E_{sup}} \times 100 \tag{5}$$

The energy loss in the osmotic engine includes the pressure drop in the tubing between the pump and the hydrogel cylinder, the pressure drop when pumping through the hydrogel in the cylinder, and the frictional force between the plunger and cylinder.

The pressure drop in the tubing is due to the friction of the fluid against the tube wall. The pressure drop in the cylindrical tubing can be estimated by the Darcy–Weisbach equation:[38,39]

$$\Delta p_t = f_D \frac{L}{2d_t} \rho v^2 \tag{6}$$

where $d_t$ is the inner tube diameter, $L$ the length of the tube, $\rho$ is the density of water (1000 kg/m$^3$), $v$ is the velocity of the flow, and $f_D$ is the Darcy friction factor. For the utilized tubing with an inner diameter of 3 mm and flow velocity of 0.0082 m/s and with a dynamic viscosity ($\mu$) of water at 25 °C of $8.9 \times 10^{-4}$ Pa·s, the Reynolds number ($Re = \rho v d_t/\mu$) is 28. This illustrates that the flow is laminar since $Re \ll 2100$.[40] Accordingly, we can utilize the Darcy friction factor $f_D = 64/Re$ for laminar flow. The Darcy–Weisbach equation can thereby be rewritten as

$$\Delta p_t = \frac{128 L \mu Q}{\pi d_t^4} \tag{7}$$

In eq 7, the pressure drop in the tubing is strongly dependent on the diameter of the tube. Accordingly, an increase in tube diameter can significantly reduce the pressure drop. The power ($P_t$) lost from the pressure drop in the tubing can be determined by

$$P_t = Q \Delta p_t \tag{8}$$

and the corresponding energy loss ($E_t$) is given by

$$E_t = t P_t \tag{9}$$

where $t$ is the time during which the liquid is pumped through the tubing.

The pressure drop in the hydrogel cylinder can be estimated as a fluid flow through a packed bed, where the pressure drop is due to friction with the hydrogel particles. The pressure drop through a packed bed in a cylinder can be described by the Ergun equation:[41]

$$\Delta p_c = H\left[\frac{150\mu(1-\varepsilon)^2 u_s}{\varepsilon^3 d_p^2} + \frac{1.75(1-\varepsilon)\rho u_s^2}{\varepsilon^3 d_p}\right] \tag{10}$$

where $H$ is the height of the gel bead column, $d_p$ is the diameter of the gel particles, and $\varepsilon$ is the volume fraction occupied by the flowing liquid. The superficial velocity, $u_s$, is given by the flow rate divided by the total cross-sectional area


https://doi.org/10.1021/acs.iecr.1c00409
Ind. Eng. Chem. Res. XXXX, XXX, XXX−XXX

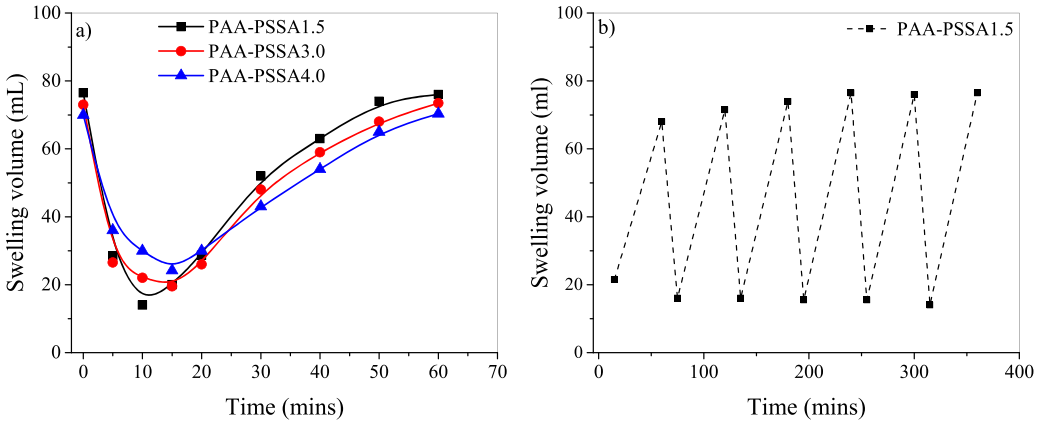


**Figure 3.** Swelling volume of hydrogels (a) during one cycle and (b) its repeatability for six consecutive cycles (maximum and minimum values for each cycle are shown).

of the cylinder: $u_s = \frac{Q}{\pi(D_c/2)^2}$, where $D_c$ is the inner diameter of the cylinder.

In addition to the energy dissipated by the pressure loss, the displacement of the piston in the hydrogel cylinder gives rise to a frictional force. The amount of energy lost to friction is dependent on a number of factors, such as the frictional coefficient between the piston and cylinder materials, the contact area between the piston and cylinder, how fast the piston moves, the presence and properties of any lubricant, and the surface morphology of the plunger and cylinder as well as the distance between them. The energy lost to friction between the piston and the cylinder will not be discussed in detail here, but it is important to keep this aspect in mind when optimizing the osmotic engine.

**2.4. Scaling Up the Osmotic Engine.** To examine the influence of the diameter of the hydrogel cylinder, a large-scale cylinder with a diameter of 240 mm with an applied pressure of 17.27 kPa was utilized. The water pump pressure was detected by a pressure sensor. Freshwater and salt water were supplied into the cylinder using four tubes with a diameter of 6 mm, with total flow rates through the four tubes of 100 mL/min and 40 mL/min in swelling and deswelling processes, respectively.

## 3. RESULTS AND DISCUSSION

**3.1. Hydrogel Swelling Ratio.** Figure 2 depicts the equilibrium swelling ratios of the semi-IPN PAA-PSSA hydrogels prepared at different cross-linking concentrations. Increasing the cross-linker concentration from 1.5 to 4.0% strongly reduces the swelling ratio. A higher cross-linker concentration shortens the distance between the cross-linking points and therefore restricts the swelling of the hydrogels.

**3.2. Mechanical Energy Extracted from Shrinking/Swelling Cycles of the Hydrogels.** The energy extracted from the PAA-PSSA hydrogels during shrinking/swelling cycles was investigated on a lab scale. A 1 h cycle of the energy recovery process was utilized. Each cycle consists of (i) shrinking when the hydrogels are exposed to a seawater-like solution (0.599 M NaCl, a flow rate of 3 mL/min) and (ii) swelling when deionized water (a flow rate of 5 mL/min) was flushed through the hydrogel. The resulting swelling volume of the hydrogels during one cycle is shown in Figure 3a. To improve the efficiency of the osmotic engine, the hydrogels are not fully swollen/deswollen during the cycles, as the last part of the swelling/shrinking process takes a relatively long time during which the volume change is small. The displacement of the plunger induced by the swelling of the hydrogels leads to an upward movement of the external weight, resulting in potential energy that can be extracted from the system. As can be seen from Figure 3a, the hydrogels shrink rapidly in the seawater-like solution and then swell to slightly different extents depending on the cross-linker density. The hydrogels exhibit good repeatability during several shrinking/swelling cycles under a constant pressure of 36.1 kPa (Figure 3b). The slight increase in swelling volume over repeated cycles is probably due to the stress of the shrinking/swelling cycles causing a gradual disassociation of hydrogen bonds within the hydrogel network.[33]

The energy from mixing solutions of different salinities was harvested through swelling/deswelling of the hydrogels in a small-size osmotic engine (Figure 1). Figure 4 illustrates the

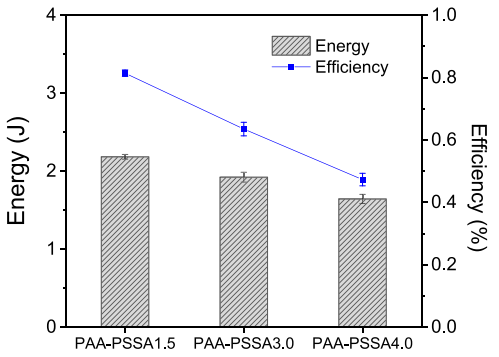


**Figure 4.** Theoretical energy and percent efficiency of the work during one cycle for a small-scale energy production system.

total recovered energy (eq 2) and the efficiency (eq 5). The energy extracted from the system and the efficiency decrease as the cross-linker concentration is raised. This is probably due to the reduced swelling ratio at higher cross-linker densities (Figure 2). The recovered energies per gram of dried hydrogel were 7.3, 3.0, and 0.8 J/g for 1.5, 3.0, and 4.0% cross-linker, respectively. For comparison, the recovered energies of other hydrogels are 3.4 J/g for poly(allylamine hydrochloride),[30] 0.83 J/g for poly(acrylic acid),[31] 120 J/g for polysulfobetaine,[32] and 13.4 J/g for poly(acrylic acid-*co*-vinylsulfonic acid) PAA/PSVA.[33] It should however be noted that the recovered energy also depends on the experimental setup, and for a


https://doi.org/10.1021/acs.iecr.1c00409
Ind. Eng. Chem. Res. XXXX, XXX, XXX−XXX

proper comparison of the different hydrogels, they should be submitted under the same experimental conditions.

**3.3. Energy Loss in the Small-Size Energy Production System.** Losing energy to friction is inevitable during the deswelling/swelling process. When the fluid flows from the pump to the energy production system, the pressure dropped both on the friction of the flow with the tube's wall in tubing and on packed-bed gel beads in the cylinder.

The pressure drop in the tubing was estimated to be 11.2 Pa during swelling and 18.7 Pa during deswelling, utilizing the Darcy–Weisbach equation (eq 7) where $d$ = 3 mm, $L$ = 0.5 m, $\rho$ = 1000 kg/m$^3$, $\mu = 8.9 \times 10^{-4}$ Pa·s, and the volumetric flow rates ($Q$) are 3 mL/min and 5 mL/min for the deswelling and swelling processes, respectively. The energy lost in the system due to the pressure drop in the tubing is calculated by eq 9, adding up for the 10 min deswelling and 50 min swelling processes. For the utilized system, the energy lost in the tubing is about 5 mJ for each cycle, which is significantly lower than the power generated by the osmotic engine (Figure 4). In order to examine how the tubing length and diameter will affect this energy loss, $E_t$ was also calculated for other tubing lengths and diameters (keeping the remaining factors constant). As can be seen from Figure 5, the energy lost in the tubing is strongly dependent on the tubing diameter, and very thin tubing should be avoided since this would significantly reduce the efficiency of the osmotic engine. The length of the tubing is less critical than the tubing diameter, but long tubing should be avoided.

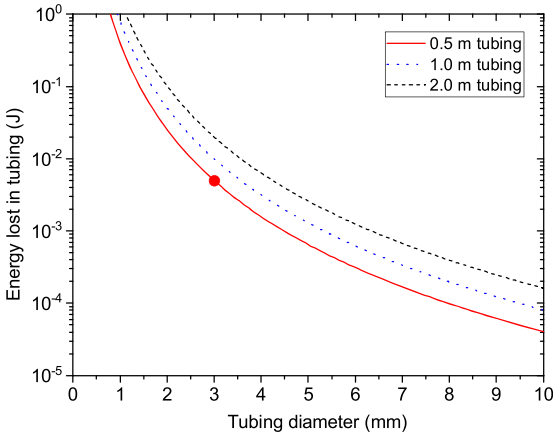


**Figure 5.** Theoretical energy lost in the tubing during the 1 h shrinking/swelling process as a function of the tubing diameter for three different tubing lengths. The red circle indicates the diameter (3 mm) and length (0.5 m) used in the experiments.

The pressure loss in the hydrogel cylinder is mainly due to the hydrogel beads, as described by the Ergun equation (eq 10). The hydrogels deswell in seawater and swell in fresh water, as shown in Figure 3a. It is difficult to accurately estimate the volume fraction occupied by the flowing liquid ($\varepsilon$). If we look at theoretical calculations, $\varepsilon$ is 0.26 for closely packed spherical particles[42,43] and about 0.36 for randomly packed monodisperse spheres.[42,44] For randomly packed ellipsoid particles, $\varepsilon$ can decrease to 0.27.[42] In addition, a polydisperse size distribution is expected to increase the packing density, which can reduce $\varepsilon$ further down to 0.2.[44] As a further complication, hydrogels are deformable, especially when subjected to an external load. In extreme cases, highly deformable particles can have $\varepsilon$ lower than 0.02.[45] For the utilized cylinder with a diameter of 4.2 cm, the superficial velocities are $3.6 \times 10^{-5}$ and $6.0 \times 10^{-5}$ m/s for flow rates of 3.0 and 5.0 mL/min, respectively. The average diameter of the swollen gel particles is estimated to be approximately 1–2 mm. The pressure loss in the system will vary through the shrinking/swelling cycle since both the size of the gel particles and the height of the gel in the cylinder change. The volume change of the hydrogel particles at different stages in the cycle is calculated, assuming that it is proportional to the volume change of the total hydrogel bulk in the cylinder. The power lost in the gel cylinder is determined by $P_g = Q\Delta p_c$. An example of the variation in $P_g$ throughout one cycle is illustrated in Figure 6. The energy lost in the hydrogel cylinder ($E_c$) during the shrinking/swelling cycle can be found by integrating the area under the curve in Figure 6.

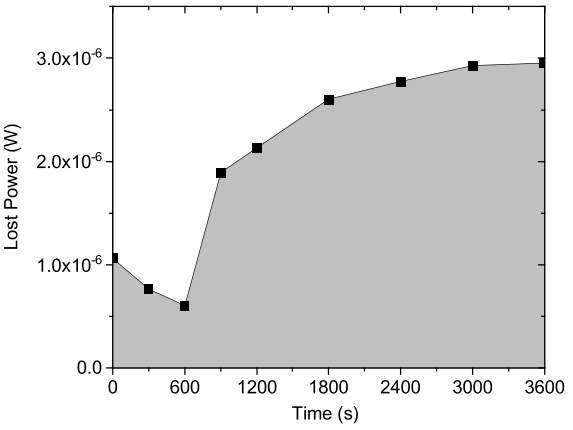


**Figure 6.** Power loss as a function of time during one shrinking/swelling cycle for PAA-PSSA1.5, assuming a swollen hydrogel particle size of 1.0 mm and $\varepsilon$ = 0.2. The energy lost during the cycle can be found by integrating the area under the curve.

If there is an ample space between the hydrogel particles (high $\varepsilon$), the liquid can easily flow through the gel, and the pressure loss will be small. However, when the voids between the gel particles are small and few (high $\varepsilon$), the pressure drop becomes significant. Figure 7 shows the energy lost by pumping through the hydrogel cylinder as a function of $\varepsilon$.

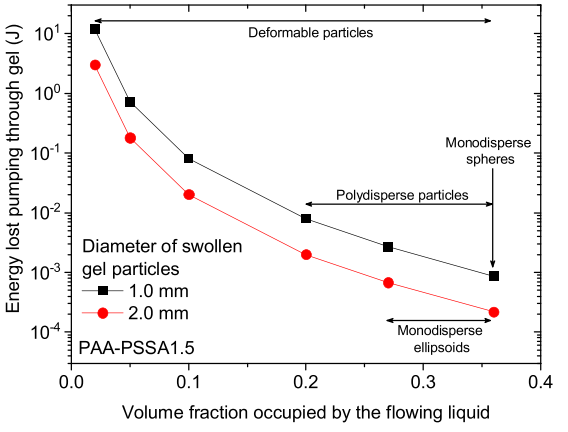


**Figure 7.** Energy lost by the pressure loss when pumping the liquid through the hydrogel column as a function of volume fraction occupied by the flowing liquid ($\varepsilon$) for two different sizes of the swollen gel particles.


https://doi.org/10.1021/acs.iecr.1c00409
Ind. Eng. Chem. Res. XXXX, XXX, XXX–XXX

Even for a polydisperse particle distribution where $\varepsilon = 0.2$, the lost energy is much smaller than the energy produced (Figure 4). However, hydrogels are soft materials that will deform under external pressure. The more the hydrogel deform, the smaller the $\varepsilon$ is.[45] When $\varepsilon$ becomes very low, the energy lost by pumping through the gel becomes a significant factor that approaches (and eventually surpass) the produced energy. It is therefore essential to utilize hydrogels with low deformation under external pressure. Increasing the cross-linking density is expected to result in stronger hydrogels with less deformation. However, high cross-linking densities will also reduce the degree of swelling (Figure 2), which might decrease the amount of energy produced by the system. Figure 7 also illustrates that increasing the size of the hydrogel particles significantly reduces the energy lost by pumping through the hydrogel cylinder. Utilizing monodisperse spherical hydrogel particles ($\varepsilon = 0.36$) is also a great advantage compared to broad particle size distribution ($\varepsilon = 0.2$).

Since the hydrogel particles are polydisperse, an estimated average size is utilized in eq 10. When comparing the hydrogels with different cross-linker concentrations, we can compare them assuming the same average diameter of either the swollen or the deswollen hydrogel particles. Since the swelling profiles are not the same for the three hydrogels (Figure 3a), this gives different results. Figure 8 illustrates that increasing the cross-linker concentration, assuming the same size of the swollen particles, decreases $E_c$ at a constant $\varepsilon$, while the trend is opposite assuming the same size of the deswollen particles. However, the effect of cross-linking density is modest for both. The opposite trends illustrate that the differences are mainly due to the size of the hydrogel particles. A lower cross-linking density has a larger size difference between the swollen and deswollen particles (Figure 2). Since larger particles reduce the energy loss (Figure 7), this causes the observed trends in Figure 8. It is however important to note that a higher cross-linker concentration will probably reduce the compressibility of the hydrogel particles, thereby increasing $\varepsilon$. This could significantly reduce the actual energy loss in the system.

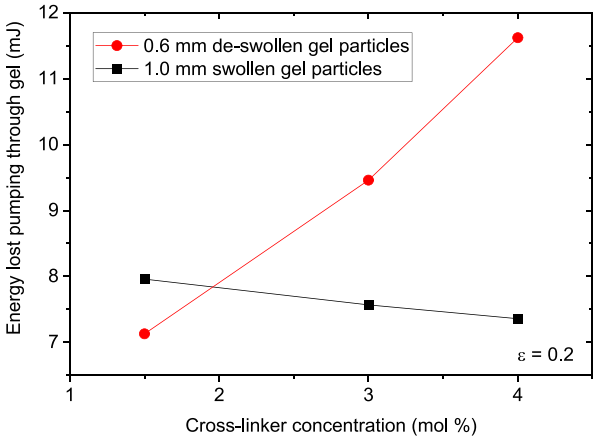


**Figure 8.** Effect of hydrogel cross-linking density on the energy lost when pumping through the hydrogel cylinder.

This energy lost by the pressure drop in the hydrogel cylinder is also dependent on the diameter of the hydrogel cylinder. If we keep the amount of hydrogel constant, increasing the diameter of the hydrogel cylinder significantly reduces the energy lost in the system (Figure 9a). This is because the height of the hydrogel within the cylinder will decrease, thereby giving less resistance to the flow. However, for scaling up, it would be natural to increase both the amount of utilized hydrogel and the flow of liquid through the system. The inset in Figure 9b shows the energy lost in the hydrogel cylinder when the volume of the swollen hydrogel is raised proportionally to the increased volume of the hydrogel cylinder while keeping the superficial velocity constant at $3.6 \times 10^{-5}$ during deswelling and $6.0 \times 10^{-5}$ during swelling processes. Under these conditions, $E_c$ increases linearly as $D_c$ becomes higher. However, increasing the amount of hydrogel utilized in the system will also result in a higher energy production. By normalizing to the energy lost per liter of swollen hydrogel (Figure 9b), it is clear that scaling up the whole system reduces the energy loss per volume unit of hydrogel. This of course raises the question of how the produced energy per volume unit of the hydrogel changes when the system is scaled up.

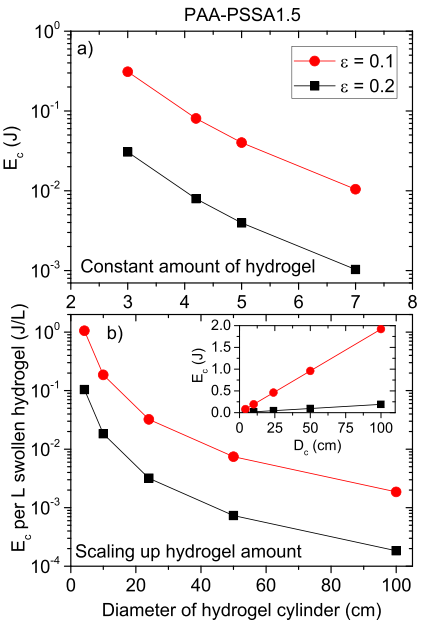


**Figure 9.** (a) Effects of increasing the diameter of the hydrogel cylinder, keeping the amount of hydrogel constant, with volumetric flow rates of 3 and 5 mL/min for the deswelling and swelling processes, respectively. (b) Effects of increasing the diameter of the hydrogel cylinder, scaling up the volume of the swollen hydrogel proportionally to the increased volume of the hydrogel cylinder and keeping the superficial velocity constant at $3.6 \times 10^{-5}$ and $6.0 \times 10^{-5}$ m/s for the deswelling and swelling processes, respectively. The diameter of the swollen hydrogel particles is set as 1.0 mm.

**3.4. Scaling Up the Osmotic Engine.** In order to examine scaling up of the osmotic engine in more detail, a system utilizing a 240 mm hydrogel cylinder was built up. Utilizing about 3 L of fully swollen PAA-PSSA1.5 hydrogel, the energy produced is about 31 J during one cycle (eq 2) for this larger system. With the utilized tubing, the pressure loss in the tubing is about 5% of the produced energy. Utilizing a larger tubing diameter is an easy measure to reduce this energy loss. The measured pressure applied to keep the desired flow rates of the freshwater and saltwater is shown in Figure 10. The pump needs to supply a significantly higher pressure during the swelling process to compensate for the pressure drop in the system. A corresponding pressure drop was not evident for the deswelling process since the osmotic engine is designed to apply a much lower pressure on the hydrogels during the


https://doi.org/10.1021/acs.iecr.1c00409
Ind. Eng. Chem. Res. XXXX, XXX, XXX−XXX

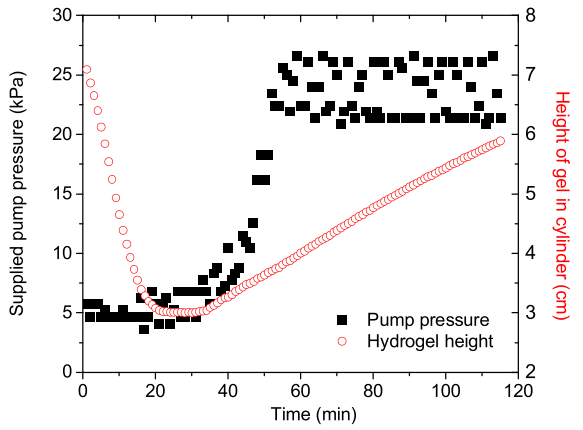


**Figure 10.** Measured pressure of the pump supplying water that is flowing through the hydrogel and the height of the hydrogel in the cylinder as a function of time during one deswelling/swelling cycle.

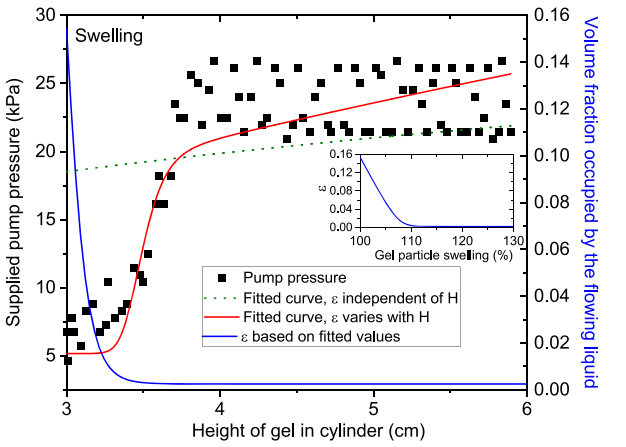


**Figure 11.** Measured pump pressure as a function of the height of the hydrogels during the swelling process together with the fitted curve according to eq 15, and $\varepsilon$ calculated based on the fitted values. The dotted line illustrates a fit to the data where $\varepsilon$ is assumed to be independent of the degree of swelling. The inset plot illustrates how $\varepsilon$ varies with the degree of swelling of the hydrogel particles.

deswelling process. This will cause less deformation of the hydrogels, resulting in a higher $\varepsilon$ and thereby a smaller pressure loss.

Since the pressure drop ($\Delta p_c$) can be calculated by the Ergun equation (eq 10), the pressure change could be used to estimate the volume fraction occupied by the flowing liquid ($\varepsilon$) by

$$p_{tot} = p_0 + \Delta p_c \tag{11}$$

where $p_{tot}$ is the measured pressure of the water pumped through the system and $p_0$ is the supplied pressure for a system without the pressure drop from the water being pumped through the hydrogel cylinder. Assuming a constant $\varepsilon$ value, the size of the hydrogel particles varies with the degree of swelling as $d_p = d_{p,ds}\left[\frac{H}{H_{ds}}\right]^{1/3}$, where $d_{p,ds}$ is the minimum size of the deswollen particles (estimated as 1 mm) and $H_{ds}$ is the height of the hydrogel in the cylinder in the deswollen state (3 cm).

However, when trying to fit the pressure change during the swelling process utilizing eq 11 (substituting in eq 10 for $\Delta p_c$ and letting $d_p$ vary with the degree of swelling), the resulting fitted curve did not even remotely follow the experimental data (dotted line in Figure 11). Since the swollen hydrogel particles are expected to have weaker mechanical properties than the corresponding deswollen particles, it is reasonable to assume that the swollen particles will deform more under the applied external pressure. A higher deformation will reduce $\varepsilon$.[45] Looking at how the pump pressure varies with the height of the hydrogel in the cylinder during the swelling process (Figure 11), it is clear that the pressure loss in the system increases sharply as the hydrogel starts to swell, before it stabilizes at high swelling degrees. Assuming that this form of the curve is due to variations of $\varepsilon$, an empirical equation for $\varepsilon$ was designed to correspond to the form of the experimental curve:

$$\varepsilon = \varepsilon_0 + [\varepsilon_\infty - \varepsilon_0]\exp\left(-\left(\frac{\tau}{H}\right)^\beta\right) \tag{12}$$

where $\varepsilon_0$ is the plateau value that $\varepsilon$ approaches when the gel is fully deswollen and $\varepsilon_\infty$ is the plateau value that $\varepsilon$ approaches when the gel is in its fully swollen state. $\tau$ is the hydrogel height where the curve starts to rise, and $\beta$ is a parameter related to how fast the values are changing during the transition.

For a system where $\varepsilon$ changes during swelling, $d_p$ will vary as

$$d_p = d_{p,ds}\left[\frac{(1-\varepsilon)H}{(1-\varepsilon_{ds})H_{ds}}\right]^{1/3} \tag{13}$$

where $\varepsilon_{ds}$ is the value of $\varepsilon$ when the hydrogel particles are in their deswollen state:

$$\varepsilon_{ds} = \varepsilon_0 + [\varepsilon_\infty - \varepsilon_0]\exp\left(-\left(\frac{\tau}{H_{ds}}\right)^\beta\right) \tag{14}$$

Combining eqs 10−14 gives

$$p_{tot} = p_0 + \frac{H}{[\varepsilon_0 - \varepsilon_0\alpha + \varepsilon_\infty\alpha]^3}\left[\frac{150\mu(1-\varepsilon_0+\varepsilon_0\alpha-\varepsilon_\infty\alpha)^2 u_s}{\left[d_{p,ds}\left[\frac{(1-\varepsilon_0+\varepsilon_0\alpha-\varepsilon_\infty\alpha)H}{(1-\varepsilon_0+\varepsilon_0\alpha_{ds}-\varepsilon_\infty\alpha_{ds})H_{ds}}\right]^{1/3}\right]^2} + \frac{1.75(1-\varepsilon_0+\varepsilon_0\alpha-\varepsilon_\infty\alpha)\rho u_s^2}{d_{p,ds}\left[\frac{(1-\varepsilon_0+\varepsilon_0\alpha-\varepsilon_\infty\alpha)H}{(1-\varepsilon_0+\varepsilon_0\alpha_{ds}-\varepsilon_\infty\alpha_{ds})H_{ds}}\right]^{1/3}}\right] \tag{15}$$

where $\alpha = \exp\left(-\left(\frac{\tau}{H}\right)^\beta\right)$ and $\alpha_{ds} = \exp\left(-\left(\frac{\tau}{H_{ds}}\right)^\beta\right)$. However, $p_0$ is not independent from the other variables, and in order to avoid overparameterization of the fitting procedure and interdependent variables, $p_0$ can be expressed as $p_0 = p_{tot,ds} - \Delta p_{c,ds}$, where $\Delta p_{c,ds}$ is the pressure drop through the deswollen hydrogel:


https://doi.org/10.1021/acs.iecr.1c00409
Ind. Eng. Chem. Res. XXXX, XXX, XXX−XXX

$$\Delta p_{c,ds} = \frac{H_{ds}}{(\varepsilon_0 - \varepsilon_0\alpha_{ds} + \varepsilon_\infty\alpha_{ds})^3}\left[\frac{150\mu(1 - \varepsilon_0 + \varepsilon_0\alpha_{ds} - \varepsilon_\infty\alpha_{ds})^2 u_s}{d_{p,ds}^2} + \frac{1.75(1 - \varepsilon_0 + \varepsilon_0\alpha_{ds} - \varepsilon_\infty\alpha_{ds})\rho u_s^2}{d_{p,ds}}\right] \quad (16)$$

and $p_{tot,ds}$ is the total pressure when pumping through the deswollen hydrogel. $p_{tot,ds}$ = 5194 Pa was estimated by using the average value of the plateau (first 30 min in Figure 10). Accordingly, the pressure in Figure 11 can be fitted as

$$p_{tot} = p_{tot,ds} - \frac{H_{ds}}{(\varepsilon_0 - \varepsilon_0\alpha_{ds} + \varepsilon_\infty\alpha_{ds})^3}\left[\frac{150\mu(1 - \varepsilon_0 + \varepsilon_0\alpha_{ds} - \varepsilon_\infty\alpha_{ds})^2 u_s}{d_{p,ds}^2} + \frac{1.75(1 - \varepsilon_0 + \varepsilon_0\alpha_{ds} - \varepsilon_\infty\alpha_{ds})\rho u_s^2}{d_{p,ds}}\right] + \frac{H}{[\varepsilon_0 - \varepsilon_0\alpha + \varepsilon_\infty\alpha]^3}\left[\frac{150\mu(1 - \varepsilon_0 + \varepsilon_0\alpha - \varepsilon_\infty\alpha)^2 u_s}{\left[d_{p,ds}\left[\frac{(1 - \varepsilon_0 + \varepsilon_0\alpha - \varepsilon_\infty\alpha)H}{(1 - \varepsilon_0 + \varepsilon_0\alpha_{ds} - \varepsilon_\infty\alpha_{ds})H_{ds}}\right]^{1/3}\right]^2} + \frac{1.75(1 - \varepsilon_0 + \varepsilon_0\alpha - \varepsilon_\infty\alpha)\rho u_s^2}{d_{p,ds}\left[\frac{(1 - \varepsilon_0 + \varepsilon_0\alpha - \varepsilon_\infty\alpha)H}{(1 - \varepsilon_0 + \varepsilon_0\alpha_{ds} - \varepsilon_\infty\alpha_{ds})H_{ds}}\right]^{1/3}}\right] \quad (17)$$

Although very complex, eq 17 only has four floating variables during the fitting procedure ($\varepsilon_0$, $\varepsilon_\infty$, $\tau$, and $\beta$). Since the fitted value of $\tau$ gave values very close to the initial height of the deswollen hydrogel (3 cm), $\tau$ was fixed at this value in order to further reduce the number of floating parameters. It should be noted that the equations are based on spherical particles, which will not be the case for deformed particles. However, the resulting apparent values are expected to give reasonable trends that can provide a better understanding of the system. As can be seen from Figure 11, the resulting fitted curve corresponds reasonably well with the experimental data. The resulting fitted values are $\varepsilon_0$ = 0.24, $\varepsilon_\infty$ = 0.025, and $\beta$ = 39, resulting in $\varepsilon_{ds}$ = 0.15. Utilizing these values, $\varepsilon$ was calculated as a function of the swelling height and the degree of swelling of the gel particles (Figure 11).

Utilizing the varying $\varepsilon$ values during the swelling process but keeping the same value of $\varepsilon$ as for the fully deswollen particles during the deswelling process (since the supplied pressure is in the same range), the power lost in the osmotic engine can be estimated more accurately (Figure 12). There is a very significant power loss during the swelling process, resulting in a total energy loss of 66 kJ.

Comparing the scaled up osmotic engine with the smaller system (Figure 13), it is clear that the smaller system produces much more energy per volume of deswollen hydrogel. Some of the challenges for the scaling up is that the produced energy goes through a maximum when the weight of the external load is increased,[30] as high weights become too heavy for the gels to lift. The differences in produced energy might therefore be caused by the two osmotic engines exposing the hydrogels to dissimilar counter pressures. Accordingly, the pressure that the gels work against in the scaled up osmotic engine needs to be optimized.

Utilizing the varying $\varepsilon$ values determined from the scaled-up osmotic engine, we can obtain better values for the energy loss in the small-scale system (assuming that $\varepsilon$ is the same for the same degree of hydrogel swelling for both). In Figure 13, the energy lost by pumping through the hydrogel (compensated for the total hydrogel volume) is significantly smaller for the large-scale system. This is mainly caused by two effects: (i) the larger cylinder diameter of the scaled-up system is expected to reduce the energy loss (Figure 9b), and (ii) the hydrogel in the smaller scale system swells about 2.7 times more than in the larger osmotic engine. Since $\varepsilon$ decreases strongly with hydrogel

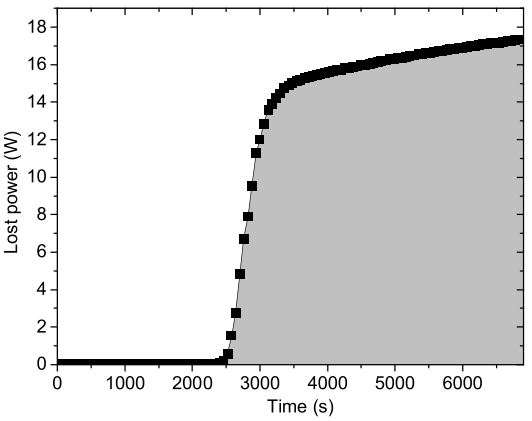


**Figure 12.** Power loss as a function of time during one shrinking/swelling cycle for PAA-PSSA1.5 in the scaled up osmotic engine. Assuming a deswollen hydrogel particle size of 1.0 mm, $\varepsilon$ is varied according to the fitted values during the swelling process, but utilizing the $\varepsilon$ value for the shrunken gel particles during the deswelling process. The energy lost during the cycle can be found by integrating the area under the curve.

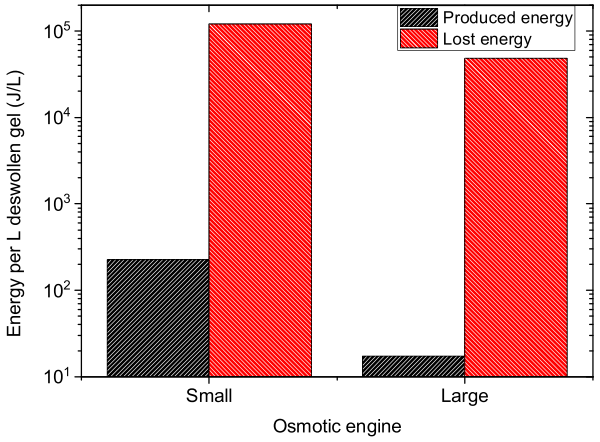


**Figure 13.** Produced energy and the energy lost by pumping through the hydrogel cylinder, both normalized for the utilized volume of the shrunken hydrogel, for the small and large osmotic engines.


https://doi.org/10.1021/acs.iecr.1c00409
Ind. Eng. Chem. Res. XXXX, XXX, XXX−XXX

swelling (inset in Figure 11), this will enhance the energy loss for the small-scale system.

Comparing the produced energy with the lost energy for the two systems (Figure 13), the energy lost is significantly larger than the energy produced for both systems. This illustrates the need for optimizing both the osmotic engines and the hydrogels for better overall efficiency. The main cause of the high energy loss is the extremely low $\varepsilon$ values for the swollen hydrogels, caused by hydrogel deformation under the applied pressure. Accordingly, designing hydrogel systems that deform less under external pressures is essential for achieving an overall energy production.

## 4. CONCLUSIONS

Utilizing hydrogels consisting of a semi-interpenetrating network of poly(4-styrene sulfonic acid-*co*-maleic acid) sodium salt and polyacrylic acid, the small-scale and large-scale osmotic engines were compared to analyze the energy loss due to the power loss in the systems. Unless very thin or extremely long tubing is utilized, the energy loss in the tubing is small compared to the energy produced by the osmotic engines.

The energy loss in the cylinder containing the hydrogel becomes smaller as the cylinder diameter is increased and when the size of the hydrogel particles is raised. However, the most pronounced effect is the volume fraction occupied by the flowing liquid ($\varepsilon$). Highly deformable particles give a very low $\varepsilon$ value and thereby a huge energy loss. Analyses of the variation of the power supplied by the liquid pump show that $\varepsilon$ varies with the degree of swelling. An empirical equation was developed to estimate how $\varepsilon$ varied through the swelling process. It was found that the hydrogel particles become much more deformable when they swell, which reduces $\varepsilon$ and causes a substantial energy loss in the system.

Stronger hydrogels that deform less under an external load will significantly reduce the amount of energy lost by pumping through the hydrogel cylinder. However, this improvement of hydrogel mechanical properties needs to be balanced against their ability to swell since reduced swelling will reduce the amount of energy produced by the system. The osmotic engine can be optimized by having a large diameter of the hydrogel cylinder, thereby reducing the height of the hydrogel through which water needs to be pumped. In addition, the pressure that the hydrogel pushes against affects both the produced energy and the energy loss and should therefore be optimized with respect to both of these factors.

## AUTHOR INFORMATION


### Corresponding Author

**Anna-Lena Kjøniksen** − *Faculty of Engineering, Østfold University College, Halden 1757, Norway;* orcid.org/0000-0003-4864-4043; Email: anna.l.kjoniksen@hiof.no

### Authors

**Tri Quang Bui** − *Faculty of Engineering, Østfold University College, Halden 1757, Norway; Department of Chemistry & Center for Pharmacy, University of Bergen, Bergen 5020, Norway*

**Vinh Duy Cao** − *Faculty of Engineering, Østfold University College, Halden 1757, Norway;* orcid.org/0000-0001-5387-3874

**Wei Wang** − *Department of Chemistry & Center for Pharmacy, University of Bergen, Bergen 5020, Norway*

**Thanh Hung Nguyen** − *Department of Construction, Energy and Materials Technology, The Arctic University of Norway, Tromsø N-9037, Norway*

Complete contact information is available at: https://pubs.acs.org/10.1021/acs.iecr.1c00409


### Notes

The authors declare no competing financial interest.

## REFERENCES


(1) Yip, N. Y.; Brogioli, D.; Hamelers, H. V. M.; Nijmeijer, K. Salinity Gradients for Sustainable Energy: Primer, Progress, and Prospects. *Environ. Sci. Technol.* **2016**, *50*, 12072−12094.

(2) Chu, S.; Majumdar, A. Opportunities and challenges for a sustainable energy future. *Nature* **2012**, *488*, 294−303.

(3) Dresselhaus, M. S.; Thomas, I. L. Alternative energy technologies. *Nature* **2001**, *414*, 332−337.

(4) Hoffert, M. I.; Caldeira, K.; Benford, G.; Criswell, D. R.; Green, C.; Herzog, H.; Jain, A. K.; Kheshgi, H. S.; Lackner, K. S.; Lewis, J. S.; Lightfoot, H. D.; Manheimer, W.; Mankins, J. C.; Mauel, M. E.; Perkins, L. J.; Schlesinger, M. E.; Volk, T.; Wigley, T. M. L. Advanced Technology Paths to Global Climate Stability: Energy for a Greenhouse Planet. *Science* **2002**, *298*, 981−987.

(5) Galán-Martín, A.; Pozo, C.; Azapagic, A.; Grossmann, I. E.; Dowelld, N. M.; Guillén-Gosálbez, G. Time for global action: an optimised cooperative approach towards effective climate change mitigation. *Energy Environ. Sci.* **2018**, *11*, 572−581.

(6) Rockström, J.; Gaffney, O.; Rogelj, J.; Meinshausen, M.; Nakicenovic, N.; Schellnhuber, H. J. A roadmap for rapid decarbonization. *Science* **2017**, *355*, 1269−1271.

(7) Norman, R. S. Water Salination: A Source of Energy. *Science* **1974**, *186*, 350−352.

(8) Pattle, R. E. Production of Electric Power by mixing Fresh and Salt Water in the Hydroelectric Pile. *Nature* **1954**, *174*, 660.

(9) Straub, A. P.; Deshmukh, A.; Elimelech, M. Pressure-retarded osmosis for power generation from salinity gradients: is it viable? *Energy Environ. Sci.* **2016**, *9*, 31−48.

(10) Ramon, G. Z.; Feinberg, B. J.; Hoek, E. M. V. Membrane-based production of salinity-gradient power. *Energy Environ. Sci.* **2011**, *4*, 4423−4434.

(11) Isaacs, J. D.; Seymour, R. J. The ocean as a power resource. *Int. J. Environ. Stud.* **1973**, *4*, 201−205.

(12) Loeb, S.; Norman, R. S. Osmotic power Plants. *Science* **1975**, *189*, 654−655.

(13) Logan, B. E.; Elimelech, M. Membrane-based processes for sustainable power generation using water. *Nature* **2012**, *488*, 313−319.

(14) Sarp, S.; Li, Z.; Saththasivam, J. Pressure Retarded Osmosis (PRO): Past experiences, current developments, and future prospects. *Desalination* **2016**, *389*, 2−14.

(15) Levenspiel, O. B.; de Nevers, N. The osmotic pump. *Science* **1974**, *183*, 157−160.

(16) Achilli, A.; Childress, A. E. Pressure retarted osmosis: From the vision of Sidney Loeb to the first prototype installation-Review. *Desalination* **2010**, *261*, 205−211.

(17) Feinberg, B. J.; Ramon, G. Z.; Hoek, E. M. V. Thermodynamic analysis of osmotic energy recovery at a reverse osmosis desalination plant. *Environ. Sci. Technol.* **2013**, *47*, 2982−2989.

(18) Post, J. W.; Hamalers, H. V. M.; Buisman, C. J. N. Energy recovery from controlled mixing salt and fresh water with a reverse electrodialysis system. *Environ. Sci. Technol.* **2008**, *42*, 5785−5790.

(19) Yip, N. Y.; Vermaas, D. A.; Nijmeijer, K.; Elimelech, M. Thermodynamic, energy efficiency, and power density analysis of reverse electrodialysis power generation with natural salinity gradients. *Environ. Sci. Technol.* **2014**, *48*, 4925−4936.

(20) Veerman, J.; Saakes, M.; Metz, S. J.; Harmsen, G. J. Reverse electrodialysis: evaluation of suitable electrode systems. *J. Appl. Electrochem.* **2010**, *40*, 1461−1474.




https://doi.org/10.1021/acs.iecr.1c00409
*Ind. Eng. Chem. Res.* XXXX, XXX, XXX−XXX

(21) Long, R.; Kuang, Z.; Liu, Z.; Liu, W. Reverse electrodialysis in bilayer nanochannels: salinity gradient-driven power generation. *Phys. Chem. Chem. Phys.* **2018**, *20*, 7295−7302.
(22) Moreno, J.; Grasman, S.; van Engelen, R.; Nijmeijer, K. Upscaling Reverse Electrodialysis. *Environ. Sci. Technol.* **2018**, *52*, 10856−10863.
(23) Zhu, X.; Kim, T.; Rahimi, M.; Gorski, C. A.; Logan, B. E. Integrating Reverse-Electrodialysis Stacks with Flow Batteries for Improved Energy Recovery from Salinity Gradients and Energy Storage. *ChemSusChem* **2017**, *10*, 797−803.
(24) Rica, R.; Ziano, R.; Salerno, D.; Mantegazza, F.; van Roij, R.; Brogioli, D. Capacitive mixing for harvesting the free energy of solutions at different concentrations. *Entropy* **2013**, *15*, 1388−1407.
(25) Brogioli, D. Extracting renewable energy from a salinity difference using a capacitor. *Phys. Rev. Lett.* **2009**, *103*, No. 058501.
(26) Sales, B. B.; Liu, F.; Schaetzle, O.; Buisman, C. J. N.; Hamelers, H. V. M. Electrochemical characterization of a supercapacitor flow cell for power production from salinity gradients. *Electrochim. Acta* **2012**, *86*, 298−304.
(27) Bijmans, M. F. M.; Burheim, O. S.; Bryjak, M.; Delgado, A.; Hack, P.; Mantegazza, F.; Tenisson, S.; Hamelers, H. V. M. Capmix-deploying capacitors for salt gradient power extraction. *Energy Procedia* **2012**, *20*, 108−115.
(28) Hatzell, M. C.; Raju, M.; Watson, V. J.; Stack, A. G.; van Duin, A. C. T.; Logan, B. E. Effect of strong acid functional groups on electrode rise potential in capacitive mixing by double layer expansion. *Environ. Sci. Technol.* **2014**, *48*, 14041−14048.
(29) Zhu, X.; Yang, W.; Hatzell, M. C.; Logan, B. E. Energy Recovery from Solutions with Different Salinities Based on Swelling and Shrinking of Hydrogels. *Environ. Sci. Technol.* **2014**, *48*, 7157−7163.
(30) Bui, T. Q.; Cao, V. D.; Do, N. B. D.; Christoffersen, T. E.; Wang, W.; Kjøniksen, A.-L. Salinity Gradient Energy from Expansion and Contraction of Poly(allylamine hydrochloride) Hydrogels. *ACS Appl. Mater.Interfaces* **2018**, *10*, 22218−22225.
(31) Arens, L.; Weißenfeld, F.; Klein, C. O.; Schlag, K.; Wilhelm, M. Osmotic Engine: Translating Osmotic Pressure into Macroscopic Mechanical Force via Poly(Acrylic Acid) Based Hydrogels. *Adv. Sci.* **2017**, *4*, 1700112.
(32) Zavahir, S.; Krupa, I.; Almaadeed, S. A.; Tkac, J.; Kasak, P. Polyzwitterionic hydrogels in engines based on the antipolyelectrolyte effect and driven by the salinity gradient. *Environ. Sci. Technol.* **2019**, *53*, 9260−9268.
(33) Bui, T. Q.; Cao, V. D.; Wang, W.; Kjøniksen, A.-L. Recovered Energy from Salinity Gradients Utilizing Various Poly(Acrylic Acid)-Based Hydrogels. *Polymer* **2021**, *13*, 645.
(34) Zhang, S.; Lin, S.; Zhao, X.; Karnik, R. Thermodynamic analysis and material design to enhance chemo-mechanical coupling in hydrogels for energy harvesting from salinity gradients. *J. Appl. Phys.* **2020**, *128*, No. 044701.
(35) Dragan, E. S. Design and applications of interpenetrating polymer network hydrogels. A review. *Chem. Eng. J.* **2014**, *243*, 572−590.
(36) Meng, Y.; Ye, L. Synthesis and swelling property of superabsorbent starch grafted with acrylic acid/2-acrylamido-2-methyl-1-propanesulfonic acid. *J. Sci. Food Agric.* **2017**, *97*, 3831−3840.
(37) Wu, M.; Kaur, P.; Yue, H.; Clemmens, A. M.; Waldeck, D. H.; Xue, C.; Liu, H. Charge density effects on the aggregation properties of poly(p-phenylene-ethynylene)-based anionic polyelectrolytes. *J. Phys. Chem. B* **2008**, *112*, 3300−3310.
(38) Brown, G. O. The History of the Darcy-Weisbach Equation for Pipe Flow Resistance. In *Environmental and Water Resources History*; American Society of Civil Engineers: 2002.
(39) Valiantzas, J. D. Explicit Power Formula for the Darcy−Weisbach Pipe Flow Equation: Application in Optimal Pipeline Design. *J. Irrig. Drain. Eng.* **2008**, *134*, 454−461.
(40) Mosetti, F. Reynold's number. In *Beaches and Coastal Geology*; Springer US: Boston, MA, 1984; pp. 686−688.
(41) Ergun, S. Fluid flow through packed columns. *Chem. Eng. Prog.* **1952**, *48*, 89−94.
(42) Donev, A.; Cisse, I.; Sachs, D.; Variano, E. A.; Stillinger, F. H.; Connelly, R.; Torquato, S.; Chaikin, P. M. Improving the Density of Jammed Disordered Packings Using Ellipsoids. *Science* **2004**, *303*, 990−993.
(43) Torquato, S.; Truskett, T. M.; Debenedetti, P. G. Is Random Close Packing of Spheres Well Defined? *Phys. Rev. Lett.* **2000**, *84*, 2064−2067.
(44) Yuan, Y.; Liu, L.; Zhuang, Y.; Jin, W.; Li, S. Coupling effects of particle size and shape on improving the density of disordered polydisperse packings. *Phys. Rev. E* **2018**, *98*, No. 042903.
(45) Cárdenas-Barrantes, M.; Cantor, D.; Barés, J.; Renouf, M.; Azéma, E. Compaction of mixtures of rigid and highly deformable particles: A micromechanical model. *Phys. Rev. E* **2020**, *102*, No. 032904.


https://doi.org/10.1021/acs.iecr.1c00409
*Ind. Eng. Chem. Res.* XXXX, XXX, XXX−XXX